

Performance of a 250L liquid Argon TPC for sub-Gev charged particle identification

J-PARC T32 collaboration

Abstract

We have constructed a LArTPC detector with fiducial mass of 150 kg as a part of the R&D program of the next generation neutrino and nucleon decay detector.

This paper describes a study of particle identification performance of the detector using well-defined charged particles (pions, kaons, and protons) with momentum of 800 MeV/c obtained at J-PARC K1.1Br beamline.

Keywords:

1. Introduction

Liquid argon TPC detectors, first studied by the ICARUS collaboration (see Ref. [1] and references therein), are continuously sensitive detectors with calorimetric and tracking capabilities. With a readout granularity that can be as low as a few mm, they allow a fine sampling down to a few percent of a radiation length, thus optimally suited for the identification of ν_e induced charged current interactions.

Large LAr TPCs, up to 100 kton size, have been proposed [2, 3, 4, 5] as far detectors in long baseline neutrino oscillation experiments for the determination of the θ_{13} mixing angle, of the neutrino mass hierarchy and ultimately for the search of CP violation in the leptonic sector.

Such detectors, if installed underground even at moderate depths, could effectively contribute to the search for proton decay [6] and act as observatories for astrophysical neutrinos [7, 8, 9].

LAr TPCs can extend the search for nucleon decay modes via modes favored by supersymmetric grand unified model up to proton lifetimes of $\sim 10^{35}$ years [6], having from 5 to 10 times the efficiency of water Cherenkov detectors for such decays. In the two body decay $p \rightarrow K^+ \bar{\nu}$, the charged kaon would be emitted with a momentum of 340 MeV/c in case of a proton at rest, and then smeared by the nucleon Fermi motion. Such kaons are not directly visible in water Cherenkov detectors due to the high momentum threshold (~ 600 MeV/c) of kaons for Cherenkov radiation in water, but they are identifiable in a LAr detector by measuring the

local energy loss along the tracks as a function of the residual range, and by their decay topology.

The construction of a tens of kton LAr TPC requires the solution of several technological problems (cryostat, LAr purification, long drifts, ionization charge readout,...) and, given the size and cost of the project, also a solid evaluation of the physics reach. In addition to the necessary R&D to extrapolate from the hundred tons scale ICARUS detector to a device 10 to 100 times larger, there are still some aspects of the behavior of particles in a LAr TPC that need to be experimentally assessed in a quantitative way in order to provide ultimate physics sensitivity estimations. We mention here energy resolutions for electromagnetic and hadronic showers, charged particle identification and electron/ π^0 separation capabilities. We believe that this kind of studies is better accomplished by exposing a LAr TPC detector to charged particle beams of known composition and momentum.

The actual performance of a LAr TPC will depend on several detector parameters, including the chosen charge readout method and the associated electronics, the readout pitch, and the resulting signal-over-noise ratio. Since several years we are working for the realization of a 100 kton-scale detector following the GLACIER concept [10], a scalable concept for a single volume LAr TPC, operated in double phase with charge extraction and amplification in the pure argon vapor phase.

At the end of 2009 we submitted a proposal [11] to the J-PARC Laboratory, focusing on the opportunities offered by a GLACIER-like detector for the exploration

of CP violation in the leptonic sector [3], on the necessary R&D and on experimental studies with prototypes exposed to charged particle beams at J-PARC. The K1.1BR beamline of the J-PARC slow extraction facility, operated in a momentum range of 200–800 MeV/c and equipped with an electro-static separator to enrich its kaon content, offers an unique opportunity for the quantitative study of particle identification in a same momentum range as kaons from proton decay.

For the first test campaign in October 2010, a 250L prototype LAr TPC, with a single readout view and operated in liquid argon phase, was exposed to the J-PARC K1.1BR beam, collecting large statistic samples of tagged kaons, pions, protons and electrons [12].

In this paper we report results from this first test exposure. A realistic simulation of the beamline and of the LAr TPC has been setup, including all detector effects like noise, drift field distortions, and LAr purity. Automated reconstruction algorithms have been developed for the reconstruction of through-going tracks, stopping tracks and particle decays. Integral collected charge distributions and differential distributions as a function of residual range are shown for all particle types.

A detailed comparison of data with simulation allows to derive the ionization charge recombination effect in LAr as a function of the stopping power. Particle identification capabilities at low momenta are also shown.

The experimental setup, including the beamline configuration and performance, is described in Section 2. The collected data sample, basic reconstruction algorithms and detector calibration are addressed in Sections 3 and 4. Section 5 describes in detail the tuning of the simulation for a realistic reproduction of the data. Data samples and comparisons with simulation for through-going pions, stopping protons and decaying kaons are shown in Sections 6, 7 and 8, respectively. Our conclusions are presented in Section 9.

2. Experimental Setup

We have described details of the experimental setup in ref.[12], and in this paper we only discuss the issues which are relevant.

2.1. K1.1Br Beamline

K1.1Br beamline is located at J-PARC slow extraction facility. It is designed and constructed for TREK experiment [13]. to obtain high intensity and high purity K^+ beam with momentum around 800 MeV/c. 30 GeV/c protons are irradiated to production target, and bending magnets and an electro-static separator (ESS)

provide excellent momentum separation and mass separation, respectively. Other than K^+ , Protons and π^+ and e^+ are also available in this beamline. While October 2010 run period, using 3.6 kW of 30 GeV/c proton on target, TREK collaboration have achieved K/π ratio of ~ 1 with Kaon rate of ~ 1 kHz. For LArTPC test, we have intentionally reduced the beam intensity to ~ 10 Hz to avoid particle overwrap, and maximum achieved K/π with this condition was $\sim 1/4$.

800 Mev/c π^+ and K^+ are passing-through the 250L TPC detector. We reduce their momentum to ~ 600 MeV/c and ~ 200 MeV/c, respectively, so that they stop inside the TPC fiducial volume. 200 MeV/c π^+ is obtained by changing the beamline optics and turning off ESS, because π^+ (and e^+) is dominant component without ESS. To obtain 600 MeV/c K^+ , a beam degrader is located at downstream of the beamline and K^+ lose its energy by ionization. We use a combination of lead glass blocks (LG) and lead brick (LB) as beam degrader with thickness of 12.5 cm and 2.5 cm, respectively.

2.2. 250L Detector

The cryostat..

The TPC we have build for this test is a simple grid chamber with active volume of $40\text{ cm} \times 40\text{ cm} \times 76\text{ cm}$.

Cathode plane and anode plane is located at the bottom and top of the field cage, respectively, and grid plane is inserted 1 cm from the anode plane. Side of the TPC is surrounded by field shapers.

The cathode and grid planes are $100\text{ }\mu\text{m}$ stainless steel wire spaced by 5 mm.

The Anode is made with PCB (printed circuit board) with readout pitch of 1 cm. Substrate of PCB is 1.6 mm FR-4 glass-reinforced epoxy and electrode is $100\text{ }\mu\text{m}$ of gold-plated copper.

The field shaper is also made with PCB

The charge

12 bit ADC with 2.5 MHz sampling frequency

2.3. Beamline Equipment

We have several beam counters to identify beam particles. There are two beam defining counters (BDC and T32 BDC) which determine acceptance of the beam, a Fitch-type Cherenkov counter (FC), and a Gas Cherenkov counter (GC), and two time of flight counters (TOF1 and TOF2).

Two TOF counters are about 3.5m apart, and time resolution is about ~ 200 ps. Figure 1 shows the flight time distribution between TOF1 and TOF2 obtained from 800 MeV/c beam particles which contain K^+ , π^+ , e^+ , and p . Three peaks which correspond to π^+e^+ , K^+ ,

and p , respectively, are well separated. FC has 4 cm of acrylic plate as Cherenkov light radiator and photo-multipliers which are aligned in circles with two different emission angles (K -ring and π -ring) as photo detector. It is designed to have maximum separation of K^+ and π^+ with momentum of 800 MeV/c. Top plot in Fig.2 shows response of FC for the 800 MeV/c beam particles. Horizontal axis and vertical axis are hit multiplicity of the π -ring and K -ring, respectively. $K^+(\pi)$ is identified as event with signal in K -ring (π -ring) but no signal in π -ring (K -ring). In case of no signals in both rings, the particle is considered as proton. Additional separation between e^+ from π^+ is provided by GC which uses atmospheric air as Cherenkov radiator. Filled histograms in bottom plot of Fig.?? shows selected K^+ event with FC information. After removing residual π^+ using TOF, K^+ sample is almost 100% purity.

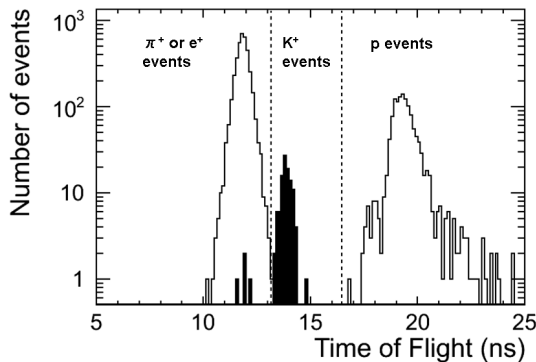


Figure 1: TOF distribution.

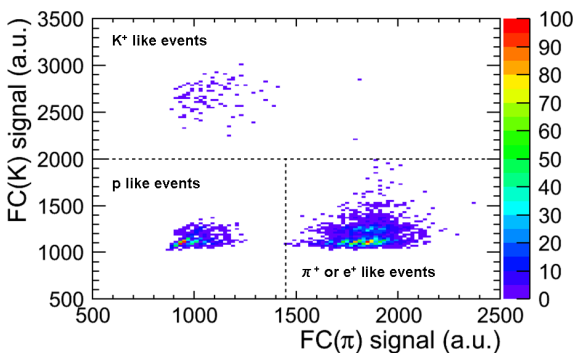


Figure 2: FC

2.4. Oct/2010 Beam Test Configuration

by using the beam counters, we define three types of triggers: (i) non-bias trigger simply requires signal in two BDCs and two TOFs; (ii) Kaon trigger requires, in addition to non-bias trigger, K identification with FC information; (iii) electron trigger requires, in addition to non-bias trigger, electron identification with GC information.

Beam Momentum

- Materials located from proton target to LArTPC detector (beam counters, beam windows, air, etc) degrade beam particle momentum
- the effect is estimated by looking at TOF of proton, average proton beam momentum is 730 MeV/c
- For other particles (K , π , e) TOF does not have enough resolution to determine momentum, and the degradation is directly estimated by counting the energy deposition to the materials using GEANT based simulation. For example Kaon momentum is xxx MeV/c on average.

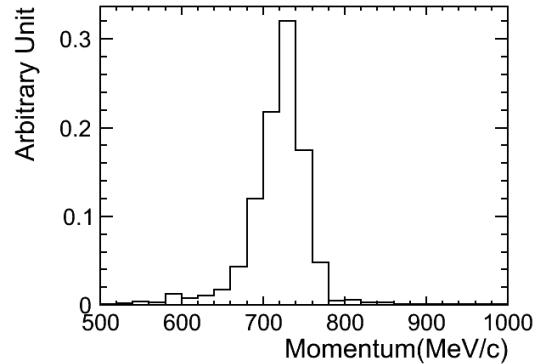


Figure 3: Top plot shows Δ TOF distribution of TOF counters with proton data, and bottom plot shows proton momentum estimated by Δ TOF of TOF counters information

We measured beam profile in front of 250LAr TPC beam window by using plastic scintillation counters. The beam is relatively narrow in vertical direction (within 5 cm), but spread in horizontal direction (~ 10 cm).

3. Data Sample and Basic Reconstruction

3.1. Collected Data

Table 1 shows list of the collected data while Oct/2010 Run. 800 MeV/c π^+ is expected to pass-through the detector as almost minimum ionizing, and

have uniform energy deposition to all the TPC channels. So this data set is useful for calibrating the detector response (See Sec. ??). 800 MeV/c proton stops after 15 cm of flight distance inside the TPC fiducial volume with relatively large dE/dx . So we use the proton data set for validation of the detector response at high dE/dx region(See Sec. 6). We have collected three different K^+ data by varying thickness of the degrader. 540, 630, 680 MeV/c correspond to the momentum degraded by 2 lead glass, 1 lead glass + 1 lead block, and 1 lead glass, respectively, and such K^+ stops after 10 cm, 50 cm, and 65 cm of flight distance inside TPC fiducial volume.

Table 1: List of collected data

Particle	Initial Momentum (MeV/c)	Number of Events
Pion	800	3,000
Proton	800	1,500
Kaon	540 (2LG)	7,000
Kaon	630 (1LG+1LB)	40,000
Kaon	680 (1LB)	35,000
electron	800	2,500
electron	200	10,000
pion	200	10,000

Top plot in Fig. 4 shows 2D display of an event taken with 800 MeV/c electron trigger. Horizontal axis corresponds to TPC channel number where zero means most upper stream strip. Since strip pitch is 1 cm, this is equivalent to distance from beam injection point in cm. Vertical axis corresponds to electron drift time in μs where $t=0$ means trigger timing. In 250L TPC, anode and cathode is located at top and bottom of the detector, respectively, drift direction is from bottom to top of the detector. With 200 V/cm of electric field, drift velocity is about 0.8 m/ms, and drift time of full detector (40 cm) is about 500 μs . Color strength of the plot corresponds to the TPC signal pulse height in ADC counts. In this event, triggered electron can be clearly identified in the center of the detector as an electromagnetic shower, while there are two other particles accidentally overlapped with the triggered electron. Track at $t=100 \mu s$ is considered as a proton which stops after 15 cm of flight distance and has large dE/dx around the stopped point. Track at $t=400 \mu s$ is considered as a pion which passes-through the detector and has uniform dE/dx over the TPC channels. Bottom plot in Fig. 4 shows a typical $K^+ \rightarrow \mu^+ \nu$ like event. We can clearly identify a kink of the track at 60 cm which is considered as stopped point of Kaon and it decays to $\mu^+ \nu$. Energy deposition of the track is about MIP at the injection point and gradually

increase towards the stopped point at 60 cm.

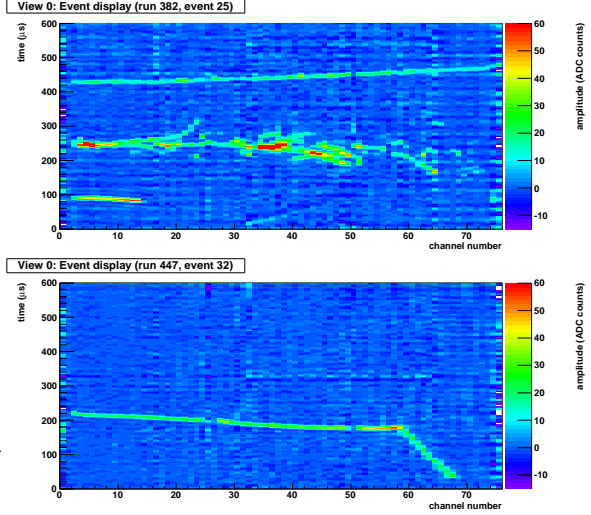


Figure 4: Event display of 800 MeV/c electron triggered event (top) accidentally overlapped with a proton and a pion, and Kaon 630 MeV/c triggered event (bottom)

3.2. Noise Reduction

Dotted line in top plots of Fig. 5 shows raw waveform of the TPC signal before applying any noise reduction. the waveform shown in this plot are channel 13 in Fig. 4 which are around the proton stopped point. Signal-to-noise ratio for this particular case is poor and pion signal which is supposed to be $t=400 \mu s$ is almost hidden by the noise. While time width of TPC signal is few μs which is determined by drift time between anode and anode-grid, dominant noise component looks higher frequency. To reduce such noises, we have applied FFT (Fast Fourier Transformation) filter to cut the high frequency component. Bottom plot in Fig. 5 shows amplitude as a function of frequency for the same event. This clearly shows dominant noise component with > 200 kHz has good separation with signal component (< 100 kHz). Solid line in top plot of Fig. 5 shows waveform after removing high frequency (> 80 kHz) component by the FFT filter. Signal-to-noise ratio is dramatically improved. On the other hand, we expect certain bias to the signal charge measurement by this filter, and it will be discussed in Section x.

3.3. Hit Finding/Clustering

After noise reduction we find signal hits and create clusters associated to single tracks. Hit is defined as bump over given threshold in a channel. Threshold of

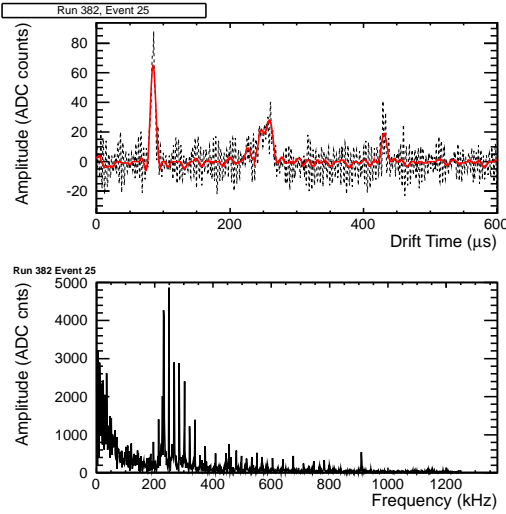


Figure 5: Top: Typical TPC signal waveform before (dotted line) and after (solid line) applying FFT low pass filter with threshold of 80 kHz, Bottom: FFT frequency amplitude distribution

hit finding is 6 ADC counts, which is about 2.5σ from typical data noise level (as shown in Fig 5) and keeping more than 99% of Kaon hit finding efficiency in simulation. ADC count distribution is fitted by Gaussian plus step function to estimate the charge of hit in $\text{ADC} \times \mu\text{s}$ unit. Fitting $\chi^2 < 3$ and $2.5 < (\text{time width of hit}) < 8 \mu\text{s}$ are required to remove noise hits further. After finding all hits in an event, we construct cluster by merging adjacent hits. The example of hit finding and clustering using Fig 4 event is shown in Fig 6, which indicates reasonable hit and cluster findings.

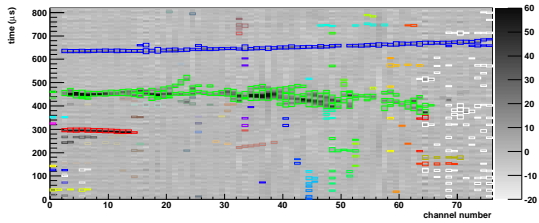


Figure 6: Example of hit finding and clustering. A colored box corresponds to a hit and colors represent different clusters.

4. Detector Calibration

4.1. Channel-by-Channel Calibration

Figure 7 shows the hit charge as a function of the TPC channel number obtained from the $800 \text{ MeV}/c \pi^+$

data. This figure is obtained from ~ 300 events of well-selected Pion passing-through the TPC. Gray-scale contours show hit charge distributions for each channel and black points correspond to average of the hit charge distribution. Although we expect the energy deposition of the through-going pion to be uniform, we observe relatively large channel dependence. This is mainly because of the distortion of the TPC drift field. We use this average charge as channel-by-channel normalization scale.

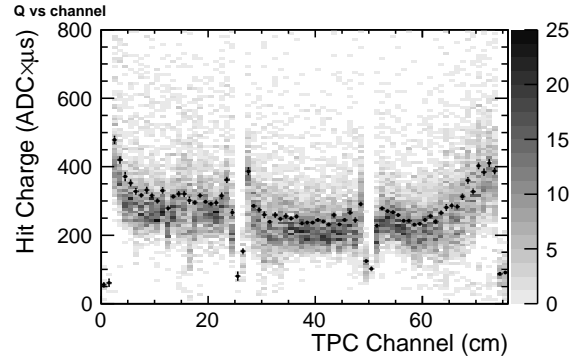


Figure 7: $800 \text{ MeV}/c$ pion average hit charge

Figure 8 shows line of force around anode calculated using a 2D FEM (Finite Element Method) package [18], where horizontal axis and vertical axis correspond to the beam line direction and the drift direction, respectively. Anode and grid are located at TPC height =20 cm and 21 cm, respectively. Top plot shows the field around corner of the TPC and bottom plot is around support frame of the grid plane. There are significant distortion of the electric field. We found this field distortion is the main cause of the non-uniformity of the TPC response.

4.2. Liquid Argon Purity

Attenuation of the drift electron depends on purity of LAr since electronegative impurities capture it [17]. Thus we need to apply correction to TPC signal charge according to the drift time. We use cosmic ray events triggered by inner PMT at off-beam timing for measuring the LAr purity, and use this to correct the beam data. Figure 9 shows an event display of typical cosmic muon event crossing TPC channels. The attenuation of readout charge depending on drift time is clearly seen in the right plot. We use multiple events to cancel Landau effect and apply channel response correction to estimate LAr purity.

We select cosmic ray event with more than 20 TPC channels which corresponds to zenith angle of more

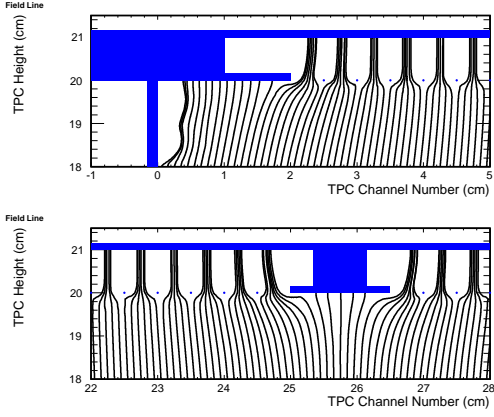


Figure 8: Line of force of the electric field obtained with 2D FEM where horizontal axis corresponds to the beam line direction, and vertical axis corresponds to drift direction.

than 27° and consistent with straight line by χ^2 fit. We fit readout charge by Landau function in each drift time bin to estimate average charge deposit. Figure 10 shows an drift electron lifetime as a function of duration after initial LAr filling. Drift electron lifetime was $600 \mu\text{s}$ at 60 hours, and $400 \mu\text{s}$ after 150 hours. The degradation is possibly due to impurity from micro leak or out-gassing penetrating faster than purification by gas recirculation. But we kept enough drift electron lifetime during data taking period. The effects from noise, field distortion, and FFT give about 10% (to be confirmed) of systematic uncertainty in LAr purity estimation.

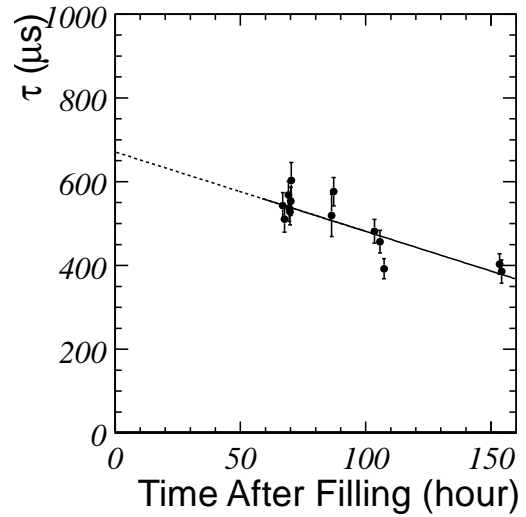


Figure 10: Drift electron lifetime as a function of duration after initial LAr filling. The lifetime is used to correct the beam data.

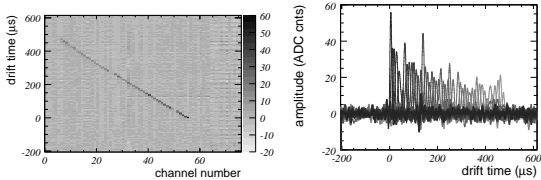


Figure 9: Left: Typical cosmic muon event crossing TPC channels. Right: Charge deposit as a function of drift time.

4.3. Signal induction

For the proper reconstruction and simulation of the signals, the electronics readout as well as the signal induction on the anode strips have to be taken into account. As described above (reference to electronics section) the shapers of the used charge sensitive preamplifiers have integration and differentiation time constants of $0.6 \mu\text{s}$ and $2.7 \mu\text{s}$, respectively. On the other hand, the signals on the different strips of the anode are induced by moving electrons, drifting between the anode-grid and the anode with a drift field of 1 kV/cm . Since this transfer time of about $5 \mu\text{s}$ is larger than the response of the electronics readout, two effects have to be taken into account: the induced unipolar signal of a strip which collects a drifting electron becomes broader,

compared to the fast electronics response, whereas on the two neighboring strips, bipolar signals are induced. Both effects were observed and verified with the weighting field method, introduced by Shockley [20].

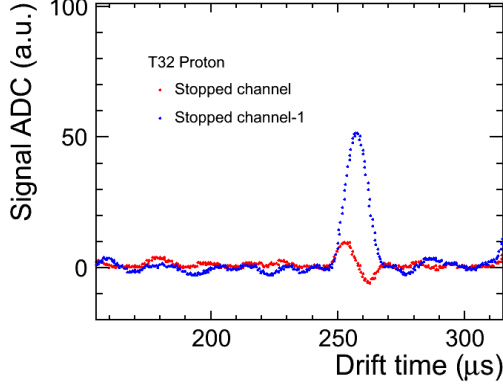


Figure 11: Left plot shows signal waveform of stopped channel and front channel, and right plot shows hit charge distribution of stopped channel

5. LArTPC Simulation

Development of the realistic simulation is one of the main task of this experiment. We try to put several effects (Field distortion, LAr purity, cross talk, etc) into this simulation, and see if the properties of LArTPC in data can be reproduced using the simulated sample.

5.1. Signal Simulation

GEANT3 is employed for simulating energy deposition of initial beam particles and secondary particles to the TPC detector and beam line counters. Maximum step of GEANT is set to 0.5 mm which is enough smaller compare to the TPC readout pitch of 1 cm. Energy cut-off for soft electron/photon emission, which is an important property to understand the performance of LArTPC, is set to 10 keV. It is minimum possible energy can be set in GEANT3. After the energy deposition, Recombination of electron and Argon ion is simulated based on the equation (Birks law),

$$Q = A \frac{Q_0}{1 + (k/E) \times (dE/dx) \times (1/\rho)} \quad (1)$$

where Q_0 is initial ionization charge, ρ is density of liquid Argon ($=1.4 \text{ g/cm}^3$), E is electric field (V/cm) electric field , and dE/dx is stopping power (MeV/g/cm^2).

Parameters of A and k are measured by ICARUS collaboration [15]. Electric field is given by 2DFEM calculation (Fig.8).

After the recombination, drift of the ionization electrons to anode is simulated using a simple step simulation with step size of 0.1 mm. Drift velocity of the ionization electron depends on the liquid Argon temperature, and the electric field. We use a measurement by ICARUS collaboration [16], and electric field in Fig.8. Typical drift velocity with 200 V/cm of the drift field and temperature of 92K is 0.8 m/ms. Diffusion of the drift electron is considered and we assume coefficient for the transverse diffusion and lateral diffusion are $9.0 \text{ mm}^2/\text{m}$ and $2.3 \text{ mm}^2/\text{m}$, respectively (need reference).

*** explanation of diffusion will be skipped ***

- Simulate Signal waveform: Gaussian

simulation of recombination, drift, waveform is done for every GEANT step, and the resulting waveform is summed up for all the particles in the event. After ending of the event process, noise waveform which describes in the next section is added to the signal waveform, and then the signal charge is digitized.

5.2. Noise Simulation

- We generate noise from FFT amplitude distribution such as in Fig.5
- By using empty event, prepare template distribution of amplitude for each channel and each frequency bin
- Obtain waveform by generating random number from the template
- Coherent noise is added board by board

Figure 12 shows simulated event of $630 \text{ MeV}/c K^+ \rightarrow \mu\nu$.

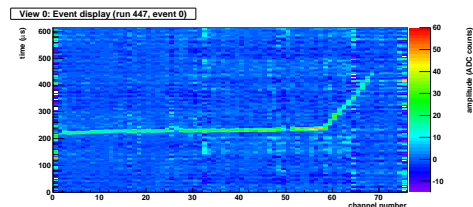


Figure 12: Event display of simulated events for $630 \text{ MeV}/c K^+$.

- Explain Landau distribution ("bare" track and "dressed" track)
- pion track (800 MeV/c) and soft electron (~ 10 keV) has different dE/dx = recombination
- Set delta-ray cut off = 10 keV in simulation, and take ICARUS measurement of recombination.
- Hit charge distribution is in good agreement between data and MC.

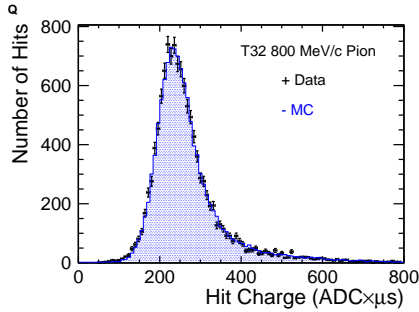


Figure 13: Hit charge distribution for 800 MeV/c through-going π^+ sample. Points and histograms correspond to data and MC, respectively

6. Stopped Proton

Proton event selection

- Protons are selected by the information of beam counters.
- Drift time of the hit at the injection point: $150\mu s$ to $300\mu s$ which corresponds with T32 BDC fiducial volume.
- Total number of hits in the cluster is greater than 5.
- Only one cluster in the event

For good proton events, we compare each parameter between data and MC. Figure 14 shows the comparison of the distribution of Hit Charge, Hit Sigma, Stopped Channel and Cluster Charge between data and MC. All four distributions of MC reproduce data well. Especially, the agreement of stopped channel distribution shows the consistent the momentum estimation by TOF information with the initial momentum of the particles injected to 250L detector.

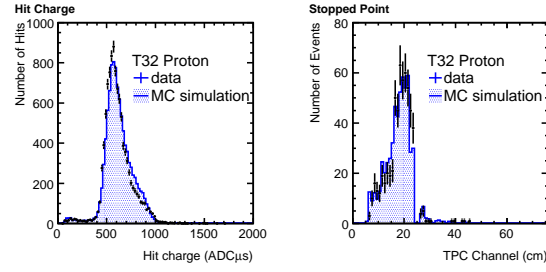


Figure 14: Hit Charge, Hit Sigma, Stopped Channel, Cluster Charge

Figure 15 shows the hit charge distribution of each distance from stopped point. Hit charge distributions of MC simulation are good agreements with data. Figure ?? shows the mean of the hit charge distribution of each distance from stopped point. MC simulation reproduce the charge response of data in high and wide dE/dx region well.

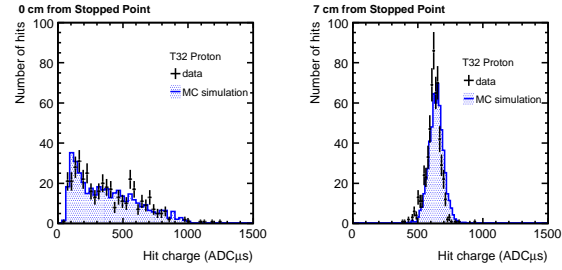


Figure 15: Hit charge distribution of each distance from stopped point

7. Stopped Kaon

- Stopping point of the Kaon is identified as kink of the track
- For example, $K \rightarrow \mu\nu$ event (Fig. 12) is composed by two tracks, Kaon and muon, and intersection of two tracks corresponds to the stopped point.
- We develop two different algorithm to identify the Kaon stopped point, Hough and Chi2.

Hough transform was invented for machine analysis of bubble chamber photographs by Paul.V.C.Hough.[19].

- Transform hit coordinates [TPC channel, drift time] into Hough space
- Find the straight line by choosing the most dense point in Hough space (= Kaon track)

- Hits associated with the first straight line are removed, and remaining hit coordinates are transformed into Hough space.
- Find second straight line using the same procedure (= Muon track)
- This procedure is repeated until number of remaining hits are less than three.
- Kaon stopped point is identified as the hit with maximum charge and around the intersection of two lines.

χ^2 method is the algorithm to Identify the kaon stopped point as the point which rapidly increase fit χ^2 to straight line.

- Starting from the most upstream hit in the cluster, fit the hits to straight line (Kaon track)
- Find the point which rapidly increase fit χ^2 to straight line.
- Starting from the most downstream hit in the cluster, fit the hits to straight line (Muon track)
- Find the point which rapidly increase fit χ^2 to straight line.
- Kaon stopped point is identified as the hit with maximum charge and around the intersection of the two lines.

Figure 16 shows Data and MC comparison for signal hit charge, signal width, decay point and total particle charge distribution. Data of signal charge and signal width are consistent with MC one in error by less than two % and data of cluster charge and primary charge are consistent with MC one in error by less than five %.

Figure 17 shows signal hit charge distribution in different distance from the stopped point. Data and MC are in good agreement.

Figure ?? shows data/MC ratio of signal hit charge distribution in different distance from the stopped point. Data of signal charge in different distance from stopped point are consistent with MC one with in 5%.

8. Recombination Factor

For the data-MC comparison, we use parameters of the recombination factor in ICARUS measurement of Ref.[15]. In this section, we measure the recombination factor using proton (and Kaon) data.

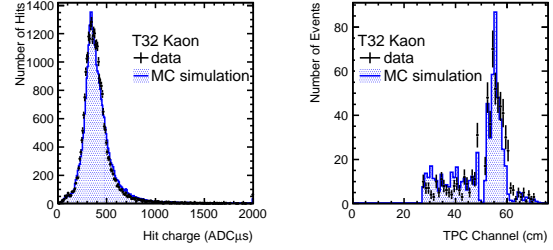


Figure 16: Data-MC comparison for hit charge, hit sigma, cluster charge, primary particle charge

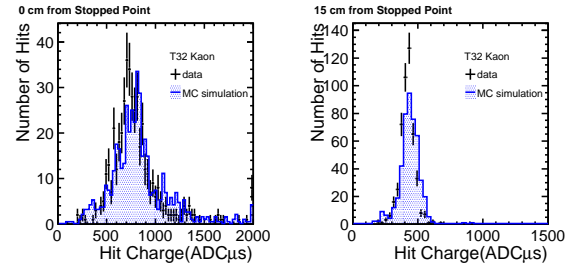


Figure 17: Data-MC comparison for hit charge distribution in different distance from the stopped point (top left: decay point, top right: decay point-5cm, bottom left: decay point-10cm, decay point-15cm)

Expression for recombination (Birks law) in Eq. 1 can be rearranged like below:

$$\frac{Q_0}{Q} = \frac{1}{A} + \frac{(k/E)(dE/dx)(1/\rho)}{A} \quad (2)$$

In this equation, the ratio of Q_0/Q has linear dependence of stopping power dE/dx , and Q from data (See Fig. ??), Q_0 and dE/dx from MC can be determined for every distance from the stopped point. By using this we are able to extract parameters A and k . Q_0 is determined from the simulation sample without recombination (Top left plot in Fig. 18), and dE/dx per an anode channel is determined with truth information of simulation (Top right plot in Fig. 18). The result of this study is shown in bottom plot of Fig18. Vertical axis is Q_0/Q , and horizontal axis is dE/dx in this figure, this plot is fitted to straight line. As a result, we obtain fitting parameter, $A = 0.832 \pm 0.009(\text{stat.}) \pm 0.006(\text{syst.})$, and $k = 0.0504 \pm 0.0010(\text{stat.}) \pm 0.0013(\text{syst.})$ [kV(g/cm²)/cm/MeV]

It confirms Birks law in the range of $4 \leq dE/dx \leq 12$ MeV/cm² and electric field of 200 V/cm is consistent with ICARUS measurement[15]. $A = 0.800 \pm 0.003$ and $k = 0.0486 \pm 0.0006$ [kV(g/cm²)/cm/MeV]

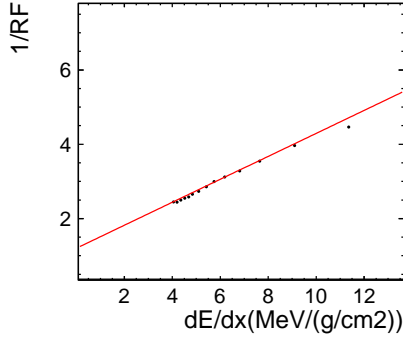


Figure 18: Q_0/Q as a function of dE/dx fitted to linear line to extract parameters of Birks law

9. Particle Identification

Put excellent plot!!!!

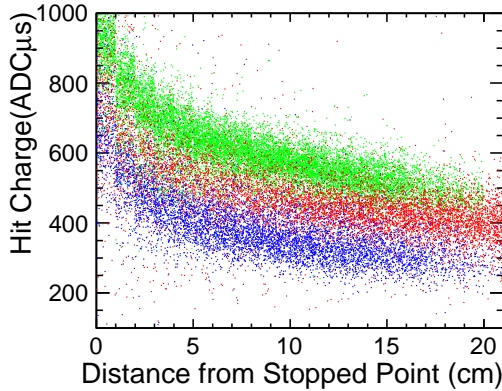


Figure 19: comparison for hit charge as a function of the distance from the stopped point for Proton, Kaon, and Pion.

10. Summary

- We have constructed 250L LArTPC
- Collected high purity Pion, Kaon, and proton sample
- Establish Kaon stopped point finding algorithm
- Develop realistic detector simulation
- Good understanding of Pion Landau distribution
- Good understanding of Proton and Kaon dE/dx

- Measurement of recombination using pi, K, and proton

References

- [1] S. Amerio *et al.* [ICARUS Collaboration], *Design, construction and tests of the ICARUS T600 detector*, Nucl. Instrum. Meth. A **527** (2004) 329.
- [2] A. Rubbia, *Experiments for CP-violation: A giant liquid argon scintillation, Cerenkov and charge imaging experiment?*, arXiv:hep-ph/0402110.
- [3] A. Badertscher *et al.*, *A Possible Future Long Baseline Neutrino and Nucleon Decay Experiment with a 100 kton Liquid Argon TPC at Okinoshima using the J-PARC Neutrino Facility*, arXiv:0804.2111 [hep-ph].
- [4] S. K. Agarwalla, T. Li and A. Rubbia, *An Incremental approach to unravel the neutrino mass hierarchy and CP violation with a long-baseline Superbeam for large θ_{13}* , arXiv:1109.6526 [hep-ph].
- [5] T. Akiri *et al.* [LBNE Collaboration], *The 2010 Interim Report of the Long-Baseline Neutrino Experiment Collaboration Physics Working Groups*, arXiv:1110.6249 [hep-ex].
- [6] A. Bueno *et al.*, *Nucleon decay searches with large liquid argon TPC detectors at shallow depths: Atmospheric neutrinos and cosmogenic backgrounds*, JHEP **0704** (2007) 041 [arXiv:hep-ph/0701101].
- [7] I. Gil Botella and A. Rubbia, *Decoupling supernova and neutrino oscillation physics with LAr TPC detectors*, JCAP **0408** (2004) 001 [arXiv:hep-ph/0404151].
- [8] A. Rubbia [ICARUS and NOE Collaborations], *ICANOE: Imaging and calorimetric neutrino oscillation experiment*, AIP Conf. Proc. **533** (2000) 220 [hep-ex/0001052].
- [9] J. Conrad, A. de Gouvea, S. Shalgar and J. Spitz, *Atmospheric Tau Neutrinos in a Multi-kiloton Liquid Argon Detector*, Phys. Rev. D **82** (2010) 093012 [arXiv:1008.2984 [hep-ph]].
- [10] A. Rubbia, *Underground Neutrino Detectors for Particle and Astroparticle Science: the Giant Liquid Argon Charge Imaging Experiment (GLACIER)*, J. Phys. Conf. Ser. **171** (2009) 012020 [arXiv:0908.1286 [hep-ph]].
- [11] A. Badertscher *et al.*, *Towards a Long Baseline Neutrino and Nucleon Decay Experiment with a next-generation 100 kton Liquid Argon TPC detector at Okinoshima and an intensity upgraded J-PARC Neutrino beam*, J-PARC Proposal P32, December 2009.
- [12] O. Araoka *et al.*, *A tagged low-momentum kaon test-beam exposure with a 250L LAr TPC (J-PARC T32)*, J. Phys. Conf. Ser. **308** (2011) 012008 [arXiv:1105.5818 [physics.ins-det]].
- [13] TREK homepage, <http://trek.kek.jp/>
- [14] S. Mihara [MEG Collaboration], Nucl. Instrum. Meth. A **518**, 45 (2004).
- [15] S. Amoruso *et al.* [ICARUS Collaboration], Nucl. Instrum. Meth. A **523**, 275 (2004).
- [16] S. Amoruso, M. Antonello, P. Aprili, F. Arneodo, A. Badertscher, B. Baibusinov, M. Baldo-Ceolin and G. Battistoni *et al.*, Nucl. Instrum. Meth. A **516**, 68 (2004).
- [17] A. Bettini *et al.*, Nucl. Instrum. Meth. A **305**, 177 (1991).
- [18] <http://www.muratasoftware.com/products/index.html>
- [19] P.V.C Hough 'Method and means for recognizing complex patterns', United States Patent Office 3069654(1962)
- [20] J. Appl. Phys. 9, 635 (1938), <http://dx.doi.org/10.1063/1.1710367>